nature photonics

REVIEW ARTICLE

PUBLISHED ONLINE: 28 APRIL 2016 | DOI: 10.1038/NPHOTON.2016.62

Perovskite photonic sources

Brandon R. Sutherland and Edward H. Sargent*

The field of solution-processed semiconductors has made great strides; however, it has yet to enable electrically driven lasers. To achieve this goal, improved materials are required that combine efficient (>50% quantum yield) radiative recombination under high injection, large and balanced charge-carrier mobilities in excess of 10 $cm^2 V^{-1} s^{-1}$, free-carrier densities greater than 10^{17} cm^{-3} and gain coefficients exceeding 10^4 cm^{-1}. Solid-state perovskites are — in addition to galvanizing the field of solar electricity — showing great promise in photonic sources, and may be the answer to realizing solution-cast laser diodes. Here, we discuss the properties of perovskites that benefit light emission, review recent progress in perovskite electroluminescent diodes and optically pumped lasers, and examine the remaining challenges in achieving continuous-wave and electrically driven lasing.

Trihalide perovskite semiconductors are an emerging class of materials that have led to great advances in the performance of solution-processed optoelectronic devices[1–4]. The bandgap is tunable through its chemical composition, allowing it to be varied across visible and near-infrared wavelengths[5]. High-quality perovskite thin films are formed at low temperature using inexpensive earth-abundant reagents. Their low Urbach energy (as small as 15 meV)[6], minimal Stokes shift (less than 20 meV)[7], high charge-carrier mobility (in excess of 10 $cm^2 V^{-1} s^{-1}$)[8], long diffusion length (up to 1 μm or even beyond)[7,9–11] and low trap density (less than 10^{16} cm^{-3})[12] have led to rapid advances in the field of solution-processed solar cell technology.

Interest in perovskites soared once their photovoltaic power conversion efficiencies ascended from 6.5% to 9.7% in 2012[13,14]. These impressive efficiencies quickly put perovskites in contention with leading third-generation solar harvesting materials, including dyes[15], organic polymers[16], colloidal quantum dots[17] and thin-film compound chalcogenides[18]. By building on pioneering advances in mesoscopic dye-sensitized solar cells, researchers greatly increased the efficiency of perovskite photovoltaics over a span of less than three years. Breakthroughs in perovskite film formation, chemical composition and optimized electrode materials increased the efficiency to 10.9%[19], 12%[20,21], 15%[22], 18.4%[23], 20.1%[24] and now to 22.1% certified[25].

Recently, researchers have explored new applications of this material, including in light-emitting diodes (LEDs) and in semiconductor optical amplifiers and lasers. We offer a critical evaluation of the prospects of perovskites in these important areas of application.

Perovskite materials for light emission

Perovskites (Fig. 1a) possess the crystal structure ABX_3, where A and B are cations jointly bound to X, an anion. Methylammonium (MA) lead trihalide perovskites have so far been the most intensively explored in optoelectronics. They have the chemical composition $CH_3NH_3PbX_nY_{3-n}$, where CH_3NH_3 and Pb are cations, and X and Y can be I, Br or Cl anions. This perovskite is a hybrid inorganic–organic direct-bandgap semiconductor, spectrally tunable through compositional control of halides. The emission ranges from 390 to 790 nm (Fig. 1b), and can be extended through cation substitution or blending. Methylammonium mixed with formamidinium extends the emission wavelength to 820 nm and has led to the most recent photovoltaic performance breakthroughs[23,24]. Perovskites of composition $MASnX_3$ have an emission wavelength tunable past 900 nm but are more sensitive to air, illumination and external bias[26].

Also extensively investigated in recent years are perovskites based on colloidal $CsPbX_3$ quantum dots. These perovskite nanoparticles offer a spectral range spanning 410–700 nm through both halide composition and quantum tuning[27]. Their narrow photoluminescence spectra, coupled with their continuous spectral tunability, enable a pure colour distribution covering a range greater than the National Television System Committee (NTSC) standard on a CIE chromaticity diagram (Fig. 1c). Some studies have shown that these perovskites exhibit less blinking (fluorescence intermittency) than other semiconductor quantum dot systems, and that the exciton is less sensitive to dot size[28].

Many of the underlying physical properties of perovskites that led to the progress in solar cell efficiencies also enable enhancements in performance of light-emitting devices. Perovskites possess a sharp optical absorption onset, with α, the absorption coefficient, exceeding 10^4 cm^{-1} near the band edge[6]. A more strongly absorbing semiconductor can efficiently convert light to electrical current, and, correspondingly, can support higher material gain in a laser. This absorption coefficient surpasses even that of GaAs, a leading semiconductor in high-performance commercial optoelectronic devices, including solar cells, LEDs and lasers.

The large mobilities in perovskites suggest promise for LEDs that can achieve high brightness at low driving voltages. In lasing applications, the low Stokes shift reduces energy lost to heat during down-conversion of the pump. A clean bandgap with minimal charge-trapping defects increases the efficiency of band-to-band radiative recombination, central to the operation of light-emitting devices. Non-radiative pathways in perovskite thin films are slow and unfavourable, even at high pump intensities, as evidenced by constant photoluminescence quantum yields near 70% at continuous-wave pump powers from 500 to 2,000 mW cm^{-2} (ref. 29) and an electroluminescence efficiency that continues to increase with injected current, owing to dominant bimolecular recombination[30].

In addition to thin-film fabrication of polycrystalline perovskites, solution-based growth of large single-crystal perovskites has recently been reported[10,11]. These single crystals offer even lower bulk defect densities, of order 10^9–10^{11} deep trap states per cubic centimetre (refs 10,31) alongside diffusion lengths exceeding 5 μm (refs 10,11) and slower non-radiative pathways[32]. As yet,

Department of Electrical and Computer Engineering, University of Toronto, 10 King's College Road, Toronto, Ontario M5S 3G4, Canada.
*e-mail: ted.sargent@utoronto.ca

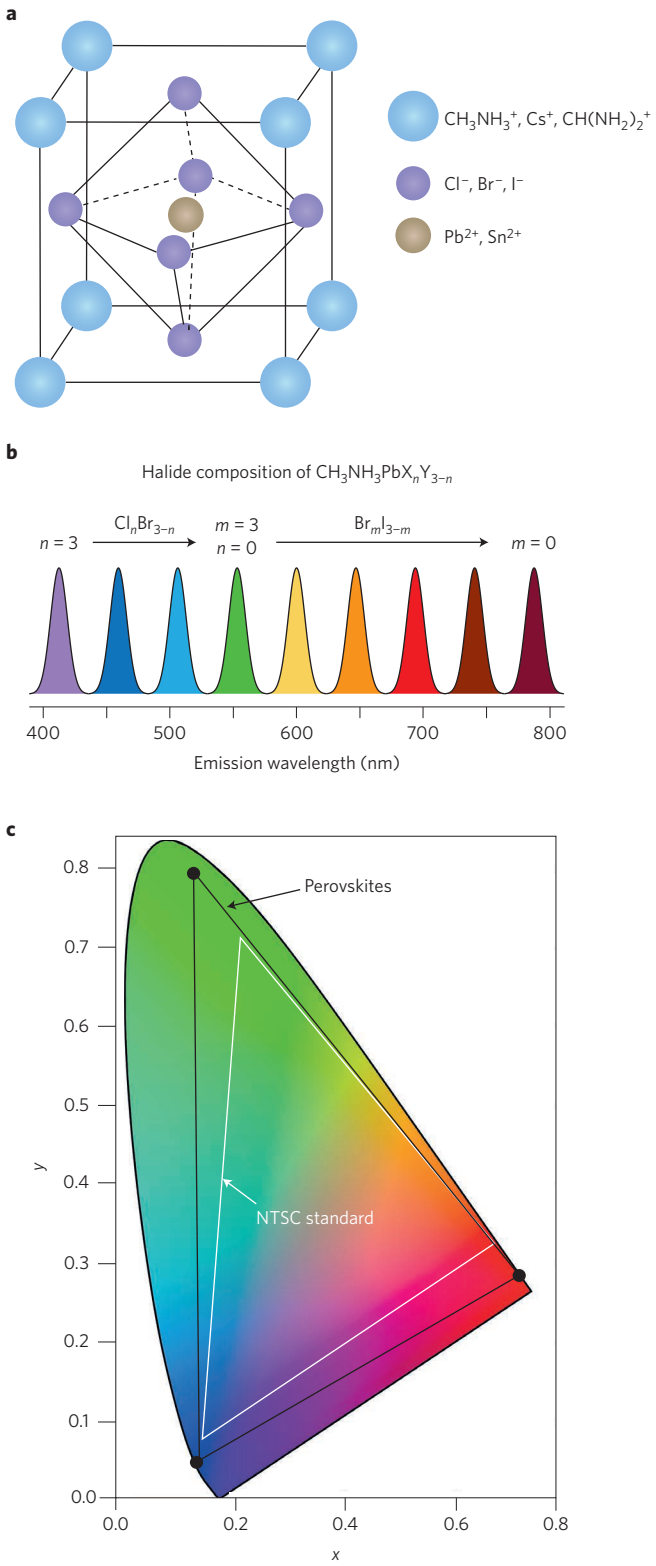

Figure 1 | Perovskite structure and emission spectrum. a, Perovskites possess the general crystal structure ABX_3. The most prevalent perovskite in optoelectronic devices is methylammonium (MA) lead trihalide, for which A = CH_3NH_3, B = Pb, and X = Cl, Br or I. **b**, Emission-wavelength tunability of $CH_3NH_3PbX_nY_{3-n}$. The emission of the $MAPbX_nY_{3-n}$ perovskite is tunable from 390 to 790 nm wavelength. **c**, CIE chromaticity diagram. Perovskites have demonstrated colour spaces covering a larger area than the National Television System Committee (NTSC) standard[27].

the large dimensions of these crystals have made them ill-suited to form optoelectronic devices based on rectifying junctions. But their applications as bulk semiconductor optical amplifiers and down-converters remain promising, and the prospect of substrate-controlled growth of patterned perovskite single crystals is a topic of intense research interest.

Perovskite light-emitting diodes

Well before halide perovskites were used for solar light harvesting, they were studied for their electroluminescence properties. Early work by Saito and colleagues in 1994 demonstrated electroluminescence from the layered $(C_6H_5C_2H_4NH_3)_2PbI_4$ perovskite, although unoptimized fabrication meant that this was only achievable at cryogenic temperatures[33].

The electronic and optical performance of solid-state perovskites is highly sensitive to the film formation method. The choice of solvent, the annealing and drying conditions, precursor choice, ratio and concentration of reagents, and deposition sequence all determine the overall quality of the film. As a result of pioneering work on perovskite photovoltaics, there now exist multiple highly tuned processing conditions for perovskite thin films. Analysis of the detailed balance of emission and absorption connects excellent photovoltaic performance with excellent LED behaviour[34]. The exceptional solar cell performance of perovskite photovoltaics, especially their high open-circuit voltage relative to their bandgap, predicts efficient operation as LEDs. After the surge in perovskite photovoltaics led by advances in thin-film development, researchers once again began investigating the prospects of these excellent solar materials in LEDs.

A typical perovksite LED consists of an intrinsic active layer in a double-heterojunction structure (Fig. 2a) with an n-type electron-transport layer (ETL) and a p-type hole-transport layer (HTL). Under forward bias, charge carriers are injected into a thin luminescent layer where they recombine radiatively, emitting light in all directions. Efficient LEDs use electrodes that readily inject carriers into the active region and prevent charges from passing through the device and quenching at contacts.

Early perovskite LEDs used emitting layers made of $CH_3NH_3PbI_3$, $CH_3NH_3PbBr_2I$ and $CH_3NH_3PbBr_3$ for near-infrared, red and green emission, respectively[30]. In the near-infrared LED, the $CH_3NH_3PbI_3$ active layer was formed between a titanium dioxide (TiO_2) ETL and a poly(9,9′-dioctylfluorene) (F8) HTL. For the larger-bandgap green and red LEDs, PEDOT:PSS was used as the HTL, and here F8 functioned as an ETL. The green LEDs reported in this work exhibited peak external quantum efficiency (EQE) of 0.1% and peak brightness of 364 cd m^{-2}. Since this work, various perovskite LEDs using different ETLs and HTLs have been reported (Fig. 2b).

The highest reported peak EQEs for perovskite LEDs are 3.5%[35] and 8.5%[36] at near-infrared and green wavelengths, respectively (Fig. 2c, left). The 8.5% value, achieved by optimizing the perovskite MABr:$PbBr_2$ precursor ratio and by pinning the perovskite grain size using molecular additives to confine the exciton, remains below the efficiencies (>20%) demonstrated for both solution-processed polymer[37] and colloidal quantum dot (CQD)[38] devices operating in the visible. The near-infrared efficiency more closely approaches the record demonstrated by CQD LEDs of 5.2%[39]. The largest peak luminance in perovskite LEDs of 20,000 cd m^{-2} is the highest reported for solution-processed green LEDs, and the peak radiance of 28 W sr^{-1} m^{-2} is a record among solution-processed emitters in the near-infrared (Fig. 2c, right)[35].

Recently, perovskite electroluminescence at blue wavelengths has been demonstrated, but with low efficiency[40,41]. This results from suboptimal injecting electrodes and band-tailing observed in chloride perovskites[42,43]. Perovskites, with complete tunability throughout the visible spectrum, are also a promising candidate for white-light LEDs. The first demonstrations of perovskite white-light

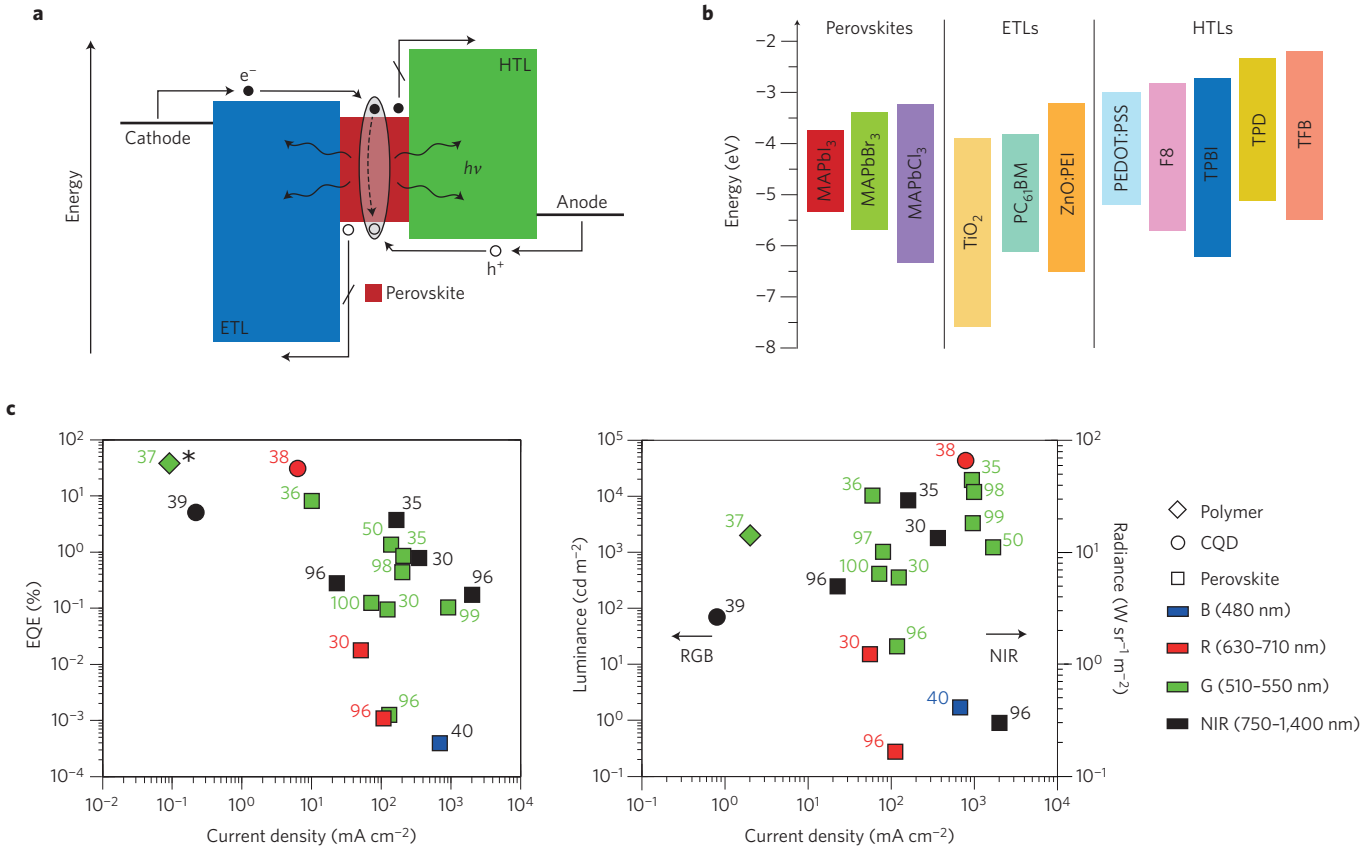

Figure 2 | Perovskite light-emitting diodes. a, General operation of perovskite LEDs. ETL, electron (e^-)-transport layer; HTL, hole (h^+)-transport layer. **b**, Energy-band alignment of methylammonium halide perovskites and the various ETLs and HTLs that have been used in reported perovskite LEDs. References: TiO_2 (ref. 30), $PC_{61}BM$ (phenyl-C_{61}-butyric acid methyl ester)[40,96], ZnO:PEI (ZnO:polyethylenimine)[35], PEDOT:PSS (poly(3,4-ethylenedioxythiophene)-poly(styrenesulfonate))[30,40,96–99], F8 (poly(9,9′-dioctylfluorene)[30,97], TPBI (1,3,5-tris(1-phenyl-1H-benzimidazol-2-yl) benzene)[36,50,100], TPD (*N*,*N*′-bis(3-methylphenyl)-*N*,*N*′-diphenylbenzidine)[96] and TFB (poly(9,9-dioctyl-fluorene-co-*N*-(4-butylphenyl)diphenylamine)[35]. **c**, External quantum efficiency (EQE, left) and brightness/radiance (right) versus current density for reported perovskite LEDs, compared with leading polymer and CQD devices. NIR, near-infrared; RGB, red/green/blue. Numbers correspond to references in which values were obtained. *This EQE is achieved from 10^{-4} to 10^{-1} mA cm^{-2}.

emission have been achieved using a 2D layered perovskite with self-trapped emissive states[44], and a blended cation mixture of tunable perovskite nanocrystals embedded in a polymer matrix[45].

The inherently low exciton binding energy in perovskites — approximately a few millielectron volts — is a limiting factor in developing high-efficiency LEDs[46]. To promote radiative recombination, thin active regions are required to confine carriers spatially. Producing ultrathin perovskite films with complete substrate coverage has proved difficult and remains an ongoing challenge on the path to higher efficiency. Stoichiometry-tuned reduced-dimensionality phenylethylammonium perovskites have recently been shown to possess higher exciton binding energies, and may show promise in light-emitting applications[47]. Perovskite nanocrystals possess larger exciton binding energies than their bulk counterparts[48]; however, initial attempts at forming LEDs from these systems have resulted in lower efficiencies than for bulk perovskites, primarily as a result of non-ideal surface passivation and poor film formation[49]. The best-performing perovskite nanocrystal LED exhibited an emission linewidth of 18 nm with peak EQE near 1% and peak brightness near 2,000 cd m^{-2}, highlighting the initial promise of these quantum-confined materials for applications in light emission[50].

The reduced Auger loss distinguish perovskites from other solution-processed materials, which are otherwise typically dominated by non-radiative losses at high carrier densities. Perovskites may therefore have distinct promise in the realization of high-intensity LEDs. But more work needs to be done to understand the root cause of the diminishing performance at higher current densities. Some reports have associated this with sample degradation due to heat generation in the active layer[30], but others argue that non-radiative recombination limits performance[51]. Given that the photoluminescence quantum yield of $CH_3NH_3PbI_3$ perovskite thin films varies considerably with sample preparation and processing conditions, it is reasonable that various perovskite LEDs exhibit different performance limitations under high injection.

Continued work on film formation, tailoring electrodes for efficient injection, and the development of new perovskite active regions engineered to promote radiative recombination will continue to lead to progress in LED efficiency and promote higher brightness at lower injection currents.

Stimulated emission in perovskites. Stimulated emission is the process by which photons induce the radiative relaxation of excited-state electrons coherently (Fig. 3a). Early evidence of stimulated emission in methylammonium lead trihalide perovskites was observed while studying the charge-transfer dynamics of efficient perovskite solar cells using ultrafast pump–probe spectroscopy[14]. Here, researchers observed negative total absorbance at energies just above the bandgap and identified it as a signature of stimulated emission, but then focused on studying the solar cell itself. As

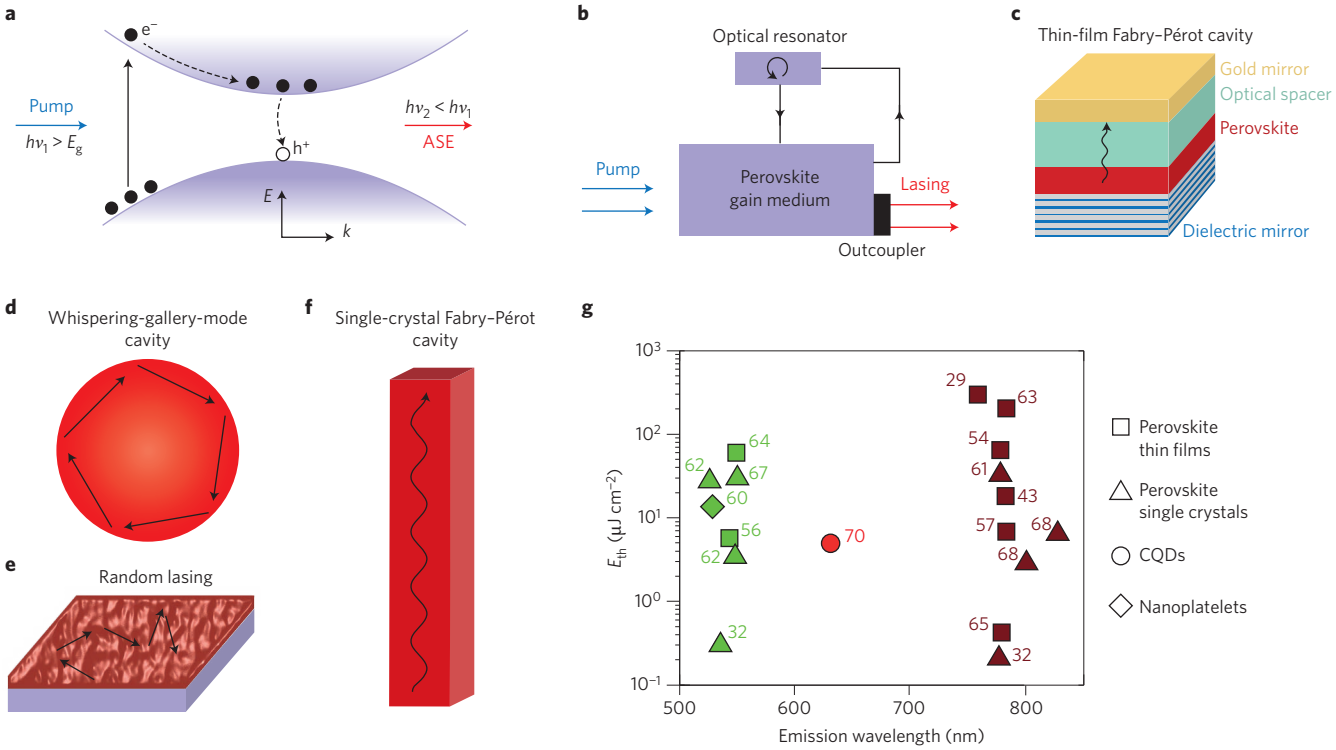

Figure 3 | Perovskite optical amplification. a, Schematic of amplified spontaneous emission (ASE) process. *ν*, photon frequency; *h*, Planck's constant; *E*, energy; E_g, bandgap; *k*, momentum. **b**, Optical amplification with a perovskite gain medium coupled with an optical cavity providing feedback, enabling lasing. **c**, Vertical surface-emitting Fabry–Pérot laser cavity with a planar perovskite gain medium[29]. **d**, Whispering-gallery-mode cavity[54,56,61,62]. **e**, Random lasing[63,64]. **f**, Perovskite single-crystal nanowire Fabry–Pérot cavity[32,66–68]. **g**, Stimulated emission threshold (E_{th}) versus emission wavelength. Numbers correspond to references in which values were obtained.

photovoltaic power conversion efficiencies soared, so too did the number of reports on perovskites for optical gain and lasing.

Optical amplification, given as gain per unit length (in cm^{-1}), can be studied by photoexciting the gain medium and measuring its spectral absorption in time. In perovskite thin films, the optical gain has been reported[52] to be as high as 3,200 ± 830 cm^{-1}. Values of this magnitude for a bulk material are comparable to single-crystal GaAs, as expected given the high absorption coefficient of perovskite. Gain has been shown to last as long as 200 ps, with a threshold near 16 μJ cm^{-2} (ref. 52).

Gain as studied using ultrafast transient absorption gives an upper limit on the net gain that can be realized in an optical amplifier. When the modes emanating from the active material propagate, they suffer additional loss per unit length. Gain offset with propagation loss is reported as the net modal gain. It is measured using the variable stripe length technique[53]. This method has been applied to perovskite thin films, and net modal gains in the range of 66–250 cm^{-1} (ref. 43), 125 cm^{-1} (ref. 54) and 6–10 cm^{-1} (ref. 55) have been reported. Caesium lead halide perovskite nanocrystals have recently emerged as an efficient solution-processed gain medium, with a net modal gain greater than 450 ± 30 cm^{-1} (ref. 56).

Using similar experimental conditions and varying the pump fluence instead of the stripe length while measuring the emitted spectral intensity profile yields the threshold for amplified spontaneous emission (ASE). Above the threshold for ASE, the luminescence spectrum greatly narrows and sharply increases in output intensity. Reported ASE thresholds range from 12 μJ cm^{-2} under 150-fs excitation[43] to 60 μJ cm^{-2} under 2-ns pumping conditions[54], and 7.6 μJ cm^{-2} at pulse durations as long as 5 ns with the aid of a liquid-crystal reflector[57]. These early values are impressive, comparable to leading values for other solution-processed materials, including long-studied semiconductor polymers[58], CQDs[59] and colloidal nanoplates[60] under similar excitation conditions.

Having demonstrated a net modal gain, perovskite researchers are exploring integration into amplification-exploiting devices: optically pumped lasers.

Perovskite lasers. Lasers require gain media capable of achieving population inversion, an optical cavity to provide feedback of coherent light, a method to outcouple this light, and net modal gain in the cavity configuration (Fig. 3b).

The first report of a trihalide perovskite laser was of a surface-emitting vertical Fabry–Pérot cavity made by coating a distributed Bragg reflector with a perovskite thin film, capped with a spacer layer and highly reflective gold mirror (Fig. 3c)[29]. The device lased when excited with intense 400-ps green laser light and produced lasing lines with a free spectral range of 9.5 THz. Since this work, there have been many new perovskite lasers using both thin films and large-dimension single crystals.

Most reported perovskite lasers have made use of whispering-gallery-mode (WGM) cavities, where optical modes guided by internal reflection around the circumference of a circular or polygonal resonator provide feedback (Fig. 3d). A spherical WGM laser was realized by conformal coating of perovskites onto glass microspheres via atomic laser deposition (ALD) — a new materials processing strategy termed perovskite ALD[54]. This fabrication approach may be of interest in the field of silicon photonics, which could benefit from monolithic integration with structured substrates and cavities. Planar WGM lasers were also developed that used perovskite nanoplates. Polygonal plates of $CH_3NH_3PbI_3$ grown by chemical vapour deposition exhibited a lasing threshold of 37 μJ cm^{-2} (ref. 61), and solution-processed single-crystal $CH_3NH_3PbBr_3$ microdisks demonstrated a threshold of 3.6 μJ cm^{-2} (ref. 62). Perovskite $CsPbX_3$

nanocrystals have also demonstrated WGM lasing with a threshold of 5 μJ cm^{-2} (ref. 56). Taking advantage of the disorder in perovskite thin films, random lasing from a $CH_3NH_3PbI_3$ microcrystal network has also been demonstrated (Fig. 3e)[63,64]. Recently, the first perovskite distributed-feedback cavity laser has been reported[65], with thresholds as low as 0.32 μJ cm^{-2}.

Single-crystal pristine and mixed iodine, bromine and chlorine perovskite nanowires have been grown and used as Fabry–Pérot optical cavities for lasing (Fig. 3f)[32,66–68]. Owing to the low trap-state density and long Auger lifetimes, the resultant lasers demonstrate lasing thresholds as low as 220 nJ cm^{-2} with lasing efficiencies approaching unity quantum yield, and quality factors of 3,600 (ref. 32). The latter two key figures of merit eclipse even the performance of epitaxial state-of-the-art GaAs–AlGaAs nanowire lasers. The exact nature of the lasing cavity in these nanowires has been shown to be dependent on sample and pump positioning, and is a competition between the lengthwise Fabry–Pérot mode and the transverse WGM[69]. The stimulated emission thresholds in perovskite nanowire single crystals are lower than some of the best values reported in colloidal nanoplatelets[60], CQDs[70] and organic polymers[58] (Fig. 3g). There have also been initial reports demonstrating more direct integration of perovskite gain media, including in amplifying waveguides[71] and in outcoupling perovskite lasers with silver nanowire plasmonic waveguides[72].

In addition to luminescent down-converters, LEDs, optical amplifiers and lasers, perovskites have also been demonstrated to be efficient nonlinear emission sources. Both $MAPbBr_3$ single-crystal nanowires[66] and $CsPbX_3$ nanocrystals[73] have exhibited multiphoton stimulated emission, with thresholds of 674 and 2,500 μJ cm^{-2}, respectively. Room-temperature single-photon emission from $CsPbX_3$ nanocrystals has also recently been demonstrated, with several benefits over traditional metal chalcogenide nonlinear emitters, such as an increased absorption cross-section, faster radiative recombination and reduced dark exciton emission[74,75].

Challenges ahead

Early organic conjugated polymer LEDs[76] and lasers[77] were demonstrated in the 1990s, pioneering a field of solution-processed semiconductor light emitters. Now, over two decades later, the field of light emission is still in search of a solution-processed material capable of electrically driven lasing. Leading contenders include organic semiconductors, inorganic colloidal nanocrystals and now perovskites. Organic semiconductors suffer from low damage thresholds, low carrier mobilities and non-radiative losses from exciton–exciton annihilation at high carrier injection[78]. Colloidal quantum dots have made impressive progress over the past two decades and carry the promise of purely inorganic films with high damage thresholds; Auger recombination needs to be overcome, however, to sustain population inversion for extended periods of time[59]. Recently, colloidal quantum wells have shown promise with an indication of continuous-wave lasing. They offer an interesting solution to the Auger recombination problem[79], but their electrical properties are largely unexplored.

Perovskites have shown initial promise in their applications for light emission. Nonetheless, much remains to be done before these materials can realize the ultimate goal of continuous-wave and, ideally, electrically excited lasing.

Increasing the duration of the excitation pulse that produces sustained inversion and lasing, ultimately towards continuous-wave operation, is a first thrust. Perovskite thin films possess a comparable Auger lifetime and stimulated emission threshold to those of colloidal nanoplatelets. Perovskite single crystals exhibit even further slowing of Auger recombination and lower thresholds. This indicates promise for perovskite lasers with reduced heat generation under high-power continuous-wave optical pumping.

So far, perovskites have achieved room-temperature ASE with 5-ns, 100-Hz pump pulses[57], and with 100-ns pump pulses at temperatures

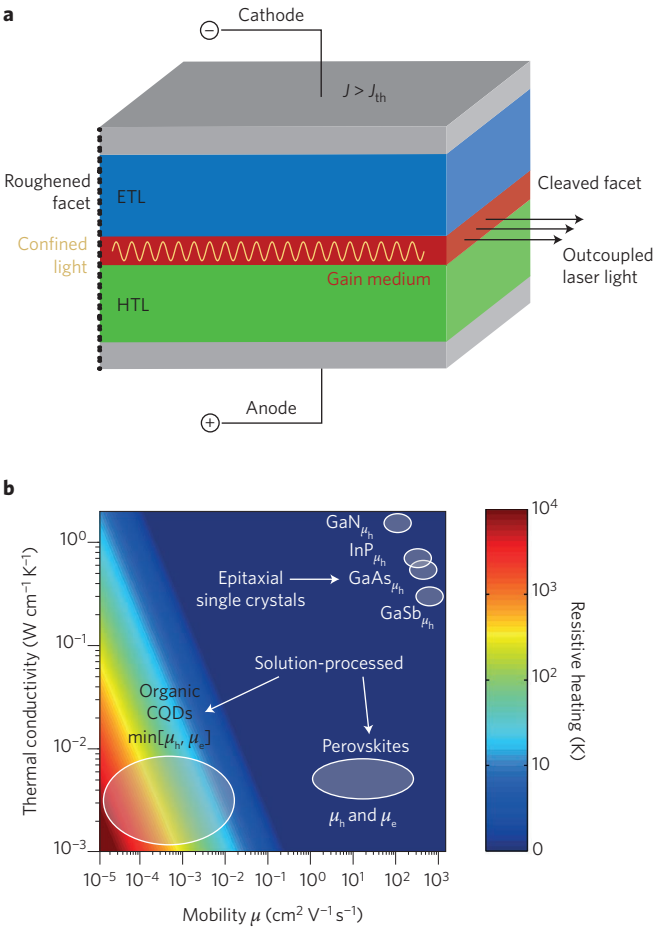

Figure 4 | Electrically injected lasing and resistive heating under current. **a**, Schematic diagram of electrically driven laser. Lasing is achieved when the injected current J is greater than the stimulated emission threshold current J_{th}. **b**, The resistive heating of a 200-nm semiconductor thin film with a carrier density of 5×10^{18} cm^{-3} under current injection of 1 kA cm^{-2}. Ellipses provide a general estimate of the limiting mobility μ in various semiconductors. μ_e, electron mobility; μ_h, hole mobility.

up to 220 K (ref. 80). Through an analysis of the feedback between the density of states at the ASE threshold and sample heating, it has been determined that the optical quality of the perovskite film and the substrate thermal conductivity are the two key parameters to further sustaining lasing over long durations of time[80]. Recently, CQDs have achieved microsecond lasing with the use of a high-thermal-conductivity substrate[81]. Such strategies have yet to be used for perovskite lasers, and processing conditions for films with high photoluminescence quantum yield have yet to be understood and reproduced consistently. Efforts towards continuous-wave lasing should aim to develop strategies to effectively convey heat from the best perovskite active materials, in order to raise the film ablation point above the threshold for stimulated emission under longer pulse durations.

To achieve electrically excited lasing, several ingredients are necessary: a high-quality gain medium with slow non-radiative decay pathways at the carrier density levels required for population inversion, large mobilities and free-carrier densities to minimize resistive heat loss, good thermal stability, a large gain cross-section at the lasing wavelength and sharp band tails marked by a low Urbach energy. Perovskites have demonstrated all of these attributes except for high carrier densities and thermal stability, making them an exciting candidate for electrically driven lasing.

A typical architecture for an edge-emitting electrically pumped diode consists of a gain medium formed between thicker n-type

electron-transport and p-type hole-transport cladding layers with lower refractive indices. This semiconductor junction is forward-biased, and a current density J is injected that is greater than the current threshold for population inversion, J_{th}. To form a laser, a cavity is required. A typical way to achieve this is by polishing one edge facet of the device and roughening the other. Emitted light from the active layer becomes trapped in the higher-refractive-index gain medium, with the polished facet acting as an outcoupler, emitting laser light (Fig. 4a).

The refractive index of hybrid organic–inorganic perovskites is typically greater than the organic ETLs and HTLs used in solution-processed LEDs. The thicknesses of these layers are typically around 50–200 nm. In a laser diode, confining light in the active region and preventing leakage of the guided mode into the metal contacts is crucial. This requires suitably thick (>500 nm) lower-refractive-index cladding layers that do not incur significant transport losses under high injection. The use of transparent top-contact conductive oxides may enable structures in which both contacts have low refractive indices, permitting the use of more conventional thin ETLs and HTLs.

There have been some promising preliminary studies, such as achieving stimulated emission in the presence of electrically quenching contacts[43,82]. The bulk defect density of perovskites is low, and these results suggest that the surface states of common ETLs and HTLs do not diminish stimulated emission efficiency in thin films.

As with continuous-wave optically pumped lasing, a principal challenge for electrical injection lasers is heat management. The large balanced electron and hole mobilities, μ_e and μ_h, in high-performance perovskite thin films, with respect to other contending technologies, correlate to reduced resistive heating under current injection. The projected temperature increase due to resistive heating, for a given mobility, μ, and thermal conductivity, K, was simulated (Fig. 4b). A threshold current density of 1 kA cm^{-2}, a typical value for compound semiconductor injection lasers, was used and was assumed to transit a 200-nm-thick semiconductor film at an ideal injected carrier density of 5×10^{18} cm^{-3}. Epitaxial single-crystal semiconductors used in commercial injection lasers, such as GaAs and InP, offer both a large K (refs 83,84) and a high limiting μ (minimum of μ_e and μ_h)[85], and do not experience any significant resistive heating under large current flow. Colloidal quantum dots[86] and organic semiconductors[87] suffer from a small K, and are limited by low mobility for at least one carrier (typically electrons for organics[88] and holes for CQDs[89]), resulting in a substantial temperature increase. Perovskites, although they have similar K values to those of other solution-processed thin films[90], possess large and balanced mobilities, so the temperature increases due to resistive heat generation are lower. These results motivate the need to solve the grand challenge of increasing the free-carrier density in perovskite materials from of order 10^{13} cm^{-3} (ref. 8) to 10^{17} cm^{-3} and beyond. These simulated resistive heat losses underestimate the actual heat generation under current injection. All energy lost through non-radiative pathways will ultimately generate heat, in addition to limiting radiative efficiency, and heat management remains a critical point of control.

An essential requirement for applications of perovskite photonic sources will be stability under the relevant injection conditions. Light-emitting perovskite devices face many of the stability concerns seen in perovskite solar cells, perhaps even more stringently as a result of the high carrier densities typically generated in these devices. Some of the strategies for photovoltaic devices hold promise for stabilizing the perovskite active medium while retaining high performance: such strategies include incorporating caesium into the lattice[91], varying the organic cation[92], using bifunctional alkylphosphonic crosslinking molecules[93] or using reduced-dimensionality perovskites (which also have the added benefit of possessing a higher exciton binding energy)[47]. Using thermally stable carrier transport layers may also improve the stability of perovskite LEDs under high carrier injection[94]. There have been some initial studies of stability in perovskite light emitters, but there is still much to learn from the large body of work on stabilizing perovskite solar cells. Stimulated emission in $MAPbI_3$ has been demonstrated over an initial 24-hour output study under continual pulsed excitation[43,54]. Nanowire lasers made of formamidinium lead halide perovskite have recently shown increased stability under continuous pulsed illumination in comparison with a $MAPbI_3$ control[68]. The lowest-threshold perovskite lasers have also demonstrated no significant variation in lasing threshold after 4–6 months of storage in inert atmosphere[32].

The toxicity of perovskite precursor materials is also an important point of consideration. All of the perovskites used so far for light-emitting applications, much like any high-performance perovskite solar cell, contain lead, a toxic substance. Implementing proper end-of-life management of any light-harvesting or light-emitting device using lead-based perovskites is critical to mitigate environmental impact. Incineration of perovskite films and subsequent recovery of the lead has been determined to be the most environmentally sustainable protocol[95]. Studies on lead-free perovskites for light emission are an encouraging yet unexplored avenue.

The photophysical properties of perovskites, and the advancement of the field of solution-processed fabrication technology, distinguish this new class of light emitters as a leading candidate for next-generation on-chip optical sources. Their promise for electrically driven lasing and their prospects as a low-cost replacement for gain media made of epitaxial III–V compound semiconductors are bright.

Received 10 June 2015; accepted 3 March 2016;
published online 28 April 2016

References

1. Park, N.-G. Organometal perovskite light absorbers toward a 20% efficiency low-cost solid-state mesoscopic solar cell. *J. Phys. Chem. Lett.* **4,** 2423–2429 (2013).
2. Kim, H.-S., Im, S. H. & Park, N.-G. Organolead halide perovskite: new horizons in solar cell research. *J. Phys. Chem. C* **118,** 5615–5625 (2014).
3. Green, M. A., Ho-Baillie, A. & Snaith, H. J. The emergence of perovskite solar cells. *Nature Photon.* **8,** 506–514 (2014).
4. Stranks, S. D. & Snaith, H. J. Metal-halide perovskites for photovoltaic and light-emitting devices. *Nature Nanotech.* **10,** 391–402 (2015).
5. Kitazawa, N., Watanabe, Y. & Nakamura, Y. Optical properties of $CH_3NH_3PbX_3$ (X = halogen) and their mixed-halide crystals. *J. Mater. Sci.* **37,** 3585–3587 (2002).
6. De Wolf, S. *et al.* Organometallic halide perovskites: sharp optical absorption edge and its relation to photovoltaic performance. *J. Phys. Chem. Lett.* **5,** 1035–1039 (2014).
7. Stranks, S. D. *et al.* Electron–hole diffusion lengths exceeding 1 micrometer in an organometal trihalide perovskite absorber. *Science* **342,** 341–344 (2013).
8. Leijtens, T. *et al.* Electronic properties of meso-superstructured and planar organometal halide perovskite films: charge trapping, photodoping, and carrier mobility. *ACS Nano* **8,** 7147–7155 (2014).
9. Xing, G. *et al.* Long-range balanced electron- and hole-transport lengths in organic-inorganic $CH_3NH_3PbI_3$. *Science* **342,** 344–347 (2013).
10. Shi, D. *et al.* Low trap-state density and long carrier diffusion in organolead trihalide perovskite single crystals. *Science* **347,** 519–522 (2015).
11. Dong, Q. *et al.* Electron–hole diffusion lengths >175 μm in solution-grown $CH_3NH_3PbI_3$ single crystals. *Science* **347,** 967–970 (2015).
12. Stranks, S. D. *et al.* Recombination kinetics in organic-inorganic perovskites: excitons, free charge, and subgap states. *Phys. Rev. Appl.* **2,** 034007 (2014).
13. Im, J.-H., Lee, C.-R., Lee, J.-W., Park, S.-W. & Park, N.-G. 6.5% efficient perovskite quantum-dot-sensitized solar cell. *Nanoscale* **3,** 4088–4093 (2011).
14. Kim, H.-S. *et al.* Lead iodide perovskite sensitized all-solid-state submicron thin film mesoscopic solar cell with efficiency exceeding 9%. *Sci. Rep.* **2,** 591 (2012).
15. Hardin, B. E., Snaith, H. J. & McGehee, M. D. The renaissance of dye-sensitized solar cells. *Nature Photon.* **6,** 162–169 (2012).
16. Li, G., Zhu, R. & Yang, Y. Polymer solar cells. *Nature Photon.* **6,** 153–161 (2012).
17. Kramer, I. J. & Sargent, E. H. The architecture of colloidal quantum dot solar cells: materials to devices. *Chem. Rev.* **114,** 863–882 (2013).

18. Suryawanshi, M. P. *et al.* CZTS based thin film solar cells: a status review. *Mater. Sci. Technol.* **28,** 98–109 (2013).
19. Lee, M. M., Teuscher, J., Miyasaka, T., Murakami, T. N. & Snaith, H. J. Efficient hybrid solar cells based on meso-superstructured organometal halide perovskites. *Science* **338,** 643–647 (2012).
20. Heo, J. H. *et al.* Efficient inorganic–organic hybrid heterojunction solar cells containing perovskite compound and polymeric hole conductors. *Nature Photon.* **7,** 486–491 (2013).
21. Noh, J. H., Im, S. H., Heo, J. H., Mandal, T. N. & Seok, S. I. Chemical management for colorful, efficient, and stable inorganic–organic hybrid nanostructured solar cells. *Nano Lett.* **13,** 1764–1769 (2013).
22. Burschka, J. *et al.* Sequential deposition as a route to high-performance perovskite-sensitized solar cells. *Nature* **499,** 316–319 (2013).
23. Jeon, N. J. *et al.* Compositional engineering of perovskite materials for high-performance solar cells. *Nature* **517,** 476–480 (2015).
24. Yang, W. S. *et al.* High-performance photovoltaic perovskite layers fabricated through intramolecular exchange. *Science* **348,** 1234–1237 (2015).
25. Research Cell Efficiency Records http://www.nrel.gov/ncpv (National Renewable Energy Laboratory, accessed 1 April 2016).
26. Hao, F., Stoumpos, C. C., Cao, D. H., Chang, R. P. H. & Kanatzidis, M. G. Lead-free solid-state organic–inorganic halide perovskite solar cells. *Nature Photon.* **8,** 489–494 (2014).
27. Protesescu, L. *et al.* Nanocrystals of cesium lead halide perovskites ($CsPbX_3$, X = Cl, Br, and I): novel optoelectronic materials showing bright emission with wide color gamut. *Nano Lett.* **15,** 3692–3696 (2015).
28. Swarnkar, A. *et al.* Colloidal $CsPbBr_3$ perovskite nanocrystals: luminescence beyond traditional quantum dots. *Angew. Chem.* **127,** 15644–15648 (2015).
29. Deschler, F. *et al.* High photoluminescence efficiency and optically pumped lasing in solution-processed mixed halide perovskite semiconductors. *J. Phys. Chem. Lett.* **5,** 1421–1426 (2014).
30. Tan, Z.-K. *et al.* Bright light-emitting diodes based on organometal halide perovskite. *Nature Nanotech.* **9,** 687–692 (2014).
31. Adinolfi, V. *et al.* The in-gap electronic state spectrum of methylammonium lead iodide single crystal perovskites. *Adv. Mater.* http://dx.doi.org/10.1002/adma.201505162 (2016).
32. Zhu, H. *et al.* Lead halide perovskite nanowire lasers with low lasing thresholds and high quality factors. *Nature Mater.* **14,** 636–642 (2015).
33. Era, M., Morimoto, S., Tsutsui, T. & Saito, S. Organic–inorganic heterostructure electroluminescent device using a layered perovskite semiconductor $(C_6H_5C_2H_4NH_3)_2PbI_4$. *Appl. Phys. Lett.* **65,** 676–678 (1994).
34. Miller, O. D., Yablonovitch, E. & Kurtz, S. R. Strong internal and external luminescence as solar cells approach the Shockley–Queisser limit. *Photovolt. IEEE J.* **2,** 303–311 (2012).
35. Wang, J. *et al.* Interfacial control toward efficient and low-voltage perovskite light-emitting diodes. *Adv. Mater.* **27,** 2311–2316 (2015).
36. Cho, H. *et al.* Overcoming the electroluminescence efficiency limitations of perovskite light-emitting diodes. *Science* **350,** 1222–1225 (2015).
37. Aizawa, N. *et al.* Solution-processed multilayer small-molecule light-emitting devices with high-efficiency white-light emission. *Nature Commun.* **5,** 5756 (2014).
38. Dai, X. *et al.* Solution-processed, high-performance light-emitting diodes based on quantum dots. *Nature* **515,** 96–99 (2014).
39. Gong, X. *et al.* Highly efficient quantum dot near-infrared light-emitting diodes. *Nature Photon.* **10,** 253–257 (2016).
40. Kumawat, N. K. *et al.* Band gap tuning of $CH_3NH_3Pb(Br_{1-x}Cl_x)_3$ hybrid perovskite for blue electroluminescence. *ACS Appl. Mater. Interfaces* **7,** 13119–13124 (2015).
41. Sadhanala, A. *et al.* Blue-green color tunable solution processable organolead chloride–bromide mixed halide perovskites for optoelectronic applications. *Nano Lett.* **15,** 6095–6101 (2015).
42. Comin, R. *et al.* Structural, optical, and electronic studies of wide-bandgap lead halide perovskites. *J. Mater. Chem. C* **3,** 8839–8843 (2015).
43. Xing, G. *et al.* Low-temperature solution-processed wavelength-tunable perovskites for lasing. *Nature Mater.* **13,** 476–480 (2014).
44. Yangui, A. *et al.* Optical investigation of broadband white-light emission in self-assembled organic–inorganic perovskite $(C_6H_{11}NH_3)_2PbBr_4$. *J. Phys. Chem. C* **119,** 23638–23647 (2015).
45. Pathak, S. *et al.* Perovskite crystals for tunable white light emission. *Chem. Mater.* **27,** 8066–8075 (2015).
46. Miyata, A. *et al.* Direct measurement of the exciton binding energy and effective masses for charge carriers in organic–inorganic tri-halide perovskites. *Nature Phys.* **11,** 582–587 (2015).
47. Quan, L. N. *et al.* Ligand-stabilized reduced-dimensionality perovskites. *J. Am. Chem. Soc.* **138,** 2649–2655 (2016).
48. Zheng, K. *et al.* Exciton binding energy and the nature of emissive states in organometal halide perovskites. *J. Phys. Chem. Lett.* **6,** 2969–2975 (2015).
49. Song, J. *et al.* Quantum dot light-emitting diodes based on inorganic perovskite cesium lead halides ($CsPbX_3$). *Adv. Mater.* **27,** 7162–7167 (2015).
50. Zhang, X. *et al.* Enhancing the brightness of cesium lead halide perovskite nanocrystal based green light-emitting devices through the interface engineering with perfluorinated ionomer. *Nano Lett.* **16,** 1415–1420 (2016).
51. Jaramillo-Quintero, O. A., Sanchez, R. S., Rincon, M. & Mora-Sero, I. Bright visible-infrared light emitting diodes based on hybrid halide perovskite with spiro-OMeTAD as a hole-injecting layer. *J. Phys. Chem. Lett.* **6,** 1883–1890 (2015).
52. Sutherland, B. R. *et al.* Perovskite thin films via atomic layer deposition. *Adv. Mater.* **27,** 53–58 (2015).
53. Shaklee, K. L. Direct determination of optical gain in semiconductor crystals. *Appl. Phys. Lett.* **18,** 475–477 (1971).
54. Sutherland, B. R., Hoogland, S., Adachi, M. M., Wong, C. T. O. & Sargent, E. H. Conformal organohalide perovskites enable lasing on spherical resonators. *ACS Nano* **8,** 10947–10952 (2014).
55. D'Innocenzo, V., Srimath Kandada, A. R., De Bastiani, M., Gandini, M. & Petrozza, A. Tuning the light emission properties by band gap engineering in hybrid lead halide perovskite. *J. Am. Chem. Soc.* **136,** 17730–17733 (2014).
56. Yakunin, S. *et al.* Low-threshold amplified spontaneous emission and lasing from colloidal nanocrystals of caesium lead halide perovskites. *Nature Commun.* **6,** 8056 (2015).
57. Stranks, S. D. *et al.* Enhanced amplified spontaneous emission in perovskites using a flexible cholesteric liquid crystal reflector. *Nano Lett.* **15,** 4935–4941 (2015).
58. Xia, R., Heliotis, G. & Bradley, D. D. C. Fluorene-based polymer gain media for solid-state laser emission across the full visible spectrum. *Appl. Phys. Lett.* **82,** 3599–3601 (2003).
59. Dang, C. *et al.* Red, green and blue lasing enabled by single-exciton gain in colloidal quantum dot films. *Nature Nanotech.* **7,** 335–339 (2012).
60. She, C. *et al.* Low-threshold stimulated emission using colloidal quantum wells. *Nano Lett.* **14,** 2772–2777 (2014).
61. Zhang, Q., Ha, S. T., Liu, X., Sum, T. C. & Xiong, Q. Room-temperature near-infrared high-Q perovskite whispering-gallery planar nanolasers. *Nano Lett.* **10,** 687–692 (2014).
62. Liao, Q. *et al.* Perovskite microdisk microlasers self-assembled from solution. *Adv. Mater.* **27,** 3405–3410 (2015).
63. Dhanker, R. *et al.* Random lasing in organo-lead halide perovskite microcrystal networks. *Appl. Phys. Lett.* **105,** 151112 (2014).
64. Liu, S. *et al.* Random lasing actions in self-assembled perovskite nanoparticles. Preprint at http://arXiv.org/abs/1512.07377 (2015).
65. Saliba, M. *et al.* Structured organic–inorganic perovskite toward a distributed feedback laser. *Adv. Mater.* **28,** 923–929 (2016).
66. Gu, Z. *et al.* Two-photon pumped lead halide perovskite nanowire lasers. Preprint at http://arXiv.org/abs/1510.03987v1 (2015).
67. Xing, J. *et al.* Vapor phase synthesis of organometal halide perovskite nanowires for tunable room-temperature nanolasers. *Nano Lett.* **15,** 4571–4577 (2015).
68. Fu, Y. *et al.* Nanowire lasers of formamidinium lead halide perovskites and their stabilized alloys with improved stability. *Nano Lett.* **16,** 1000–1008 (2016).
69. Wang, K. *et al.* Formation of single-mode laser in transverse plane of perovskite microwire via micromanipulation. *Opt. Lett.* **41,** 555–558 (2016).
70. Park, Y.-S., Bae, W. K., Baker, T., Lim, J. & Klimov, V. I. Effect of Auger recombination on lasing in heterostructured quantum dots with engineered core/shell interfaces. *Nano Lett.* **15,** 7319–7328 (2015).
71. Suárez, I., Juárez-Pérez, E. J., Bisquert, J., Mora-Seró, I. & Martínez-Pastor, J. P. Polymer/perovskite amplifying waveguides for active hybrid silicon photonics. *Adv. Mater.* **27,** 6157–6162 (2015).
72. Li, Y. J. *et al.* Output coupling of perovskite lasers from embedded nanoscale plasmonic waveguides. *J. Am. Chem. Soc.* **138,** 2122–2125 (2016).
73. Wang, Y. *et al.* Nonlinear absorption and low-threshold multiphoton pumped stimulated emission from all-inorganic perovskite nanocrystals. *Nano Lett.* **16,** 448–453 (2016).
74. Hu, F. *et al.* Superior optical properties of perovskite nanocrystals as single photon emitters. *ACS Nano* **9,** 12410–12416 (2015).
75. Park, Y.-S., Guo, S., Makarov, N. S. & Klimov, V. I. Room temperature single-photon emission from individual perovskite quantum dots. *ACS Nano* **9,** 10386–10393 (2015).
76. Burroughes, J. H. *et al.* Light-emitting diodes based on conjugated polymers. *Nature* **347,** 539–541 (1990).
77. Tessler, N., Denton, G. J. & Friend, R. H. Lasing from conjugated-polymer microcavities. *Nature* **382,** 695–697 (1996).
78. Grivas, C. & Pollnau, M. Organic solid-state integrated amplifiers and lasers. *Laser Photon. Rev.* **6,** 419–462 (2012).
79. Grim, J. Q. *et al.* Continuous-wave biexciton lasing at room temperature using solution-processed quantum wells. *Nature Nanotech.* **9,** 891–895 (2014).
80. Cadelano, M. *et al.* Can trihalide lead perovskites support continuous wave lasing? *Adv. Opt. Mater.* **3,** 1557–1564 (2015).

81. Adachi, M. M. *et al.* Microsecond-sustained lasing from colloidal quantum dot solids. *Nature Commun.* **6,** 8694 (2015).
82. Yuan, F. *et al.* Electric field-modulated amplified spontaneous emission in organo-lead halide perovskite $CH_3NH_3PbI_3$. *Appl. Phys. Lett.* **107,** 261106 (2015).
83. Voinigescu, S. *High-Frequency Integrated Circuits* (Cambridge Univ. Press, 2013).
84. Morkoc, H. *Handbook of Nitride Semiconductors and Devices* Vol. 1 (Wiley-VCH, 2008).
85. Palankovski, V. & Quay, R. *Analysis and Simulation of Heterostructure Devices* (Springer, 2004).
86. Ong, W.-L., Rupich, S. M., Talapin, D. V., McGaughey, A. J. H. & Malen, J. A. Surface chemistry mediates thermal transport in three-dimensional nanocrystal arrays. *Nature Mater.* **12,** 410–415 (2013).
87. Guo, Z. *et al.* Thermal conductivity of organic bulk heterojunction solar cells: an unusual binary mixing effect. *Phys. Chem. Chem. Phys.* **16,** 26359–26364 (2014).
88. Köhler, A. Organic semiconductors: no more breaks for electrons. *Nature Mater.* **11,** 836–837 (2012).
89. Yazdani, N., Bozyigit, D., Yarema, O., Yarema, M. & Wood, V. Hole mobility in nanocrystal solids as a function of constituent nanocrystal size. *J. Phys. Chem. Lett.* **5,** 3522–3527 (2014).
90. Pisoni, A. *et al.* Ultra-low thermal conductivity in organic–inorganic hybrid perovskite $CH_3NH_3PbI_3$. *J. Phys. Chem. Lett.* **5,** 2488–2492 (2014).
91. McMeekin, D. P. *et al.* A mixed-cation lead mixed-halide perovskite absorber for tandem solar cells. *Science* **351,** 151–155 (2016).
92. Mei, A. *et al.* A hole-conductor-free, fully printable mesoscopic perovskite solar cell with high stability. *Science* **345,** 295–298 (2014).
93. Li, X. *et al.* Improved performance and stability of perovskite solar cells by crystal crosslinking with alkylphosphonic acid ω-ammonium chlorides. *Nature Chem.* **7,** 703–711 (2015).
94. Xu, J. *et al.* Crosslinked remote-doped hole-extracting contacts enhance stability under accelerated lifetime testing in perovskite solar cells. *Adv. Mater.* **28,** 2807–2815 (2016).
95. Serrano-Lujan, L. *et al.* Tin- and lead-based perovskite solar cells under scrutiny: an environmental perspective. *Adv. Energy Mater.* **5,** 1501119 (2015).
96. Kumawat, N. K., Dey, A., Narasimhan, K. L. & Kabra, D. Near infrared to visible electroluminescent diodes based on organometallic halide perovskites: structural and optical investigation. *ACS Photon.* **2,** 349–354 (2015).
97. Li, G. *et al.* Efficient light-emitting diodes based on nanocrystalline perovskite in a dielectric polymer matrix. *Nano Lett.* **15,** 2640–2644 (2015).
98. Ling, Y. *et al.* Bright light-emitting diodes based on organometal halide perovskite nanoplatelets. *Adv. Mater.* **28,** 305–311 (2016).
99. Yu, J. C., Kim, D. B., Jung, E. D., Lee, B. R. & Song, M. H. High-performance perovskite light-emitting diodes via morphological control of perovskite films. *Nanoscale* **8,** 7036–7042 (2016).
100. Kim, Y.-H. *et al.* Multicolored organic/inorganic hybrid perovskite light-emitting diodes. *Adv. Mater.* **27,** 1248–1254 (2015).

Acknowledgements

The authors thank S. Hoogland, O. Voznyy, D. Sellan, A. Jain, G. Walters and Z. Yang for helpful discussions throughout the writing of this manuscript. The authors acknowledge support from Toyota Motors Europe.

Additional information

Reprints and permissions information is available online at www.nature.com/reprints. Correspondence should be addressed to E.H.S.

Competing financial interests

The authors declare no competing financial interests.